ISSN 1726-5749

SENSORS & TRANSDUCERS

vol. 5 Special 3/09

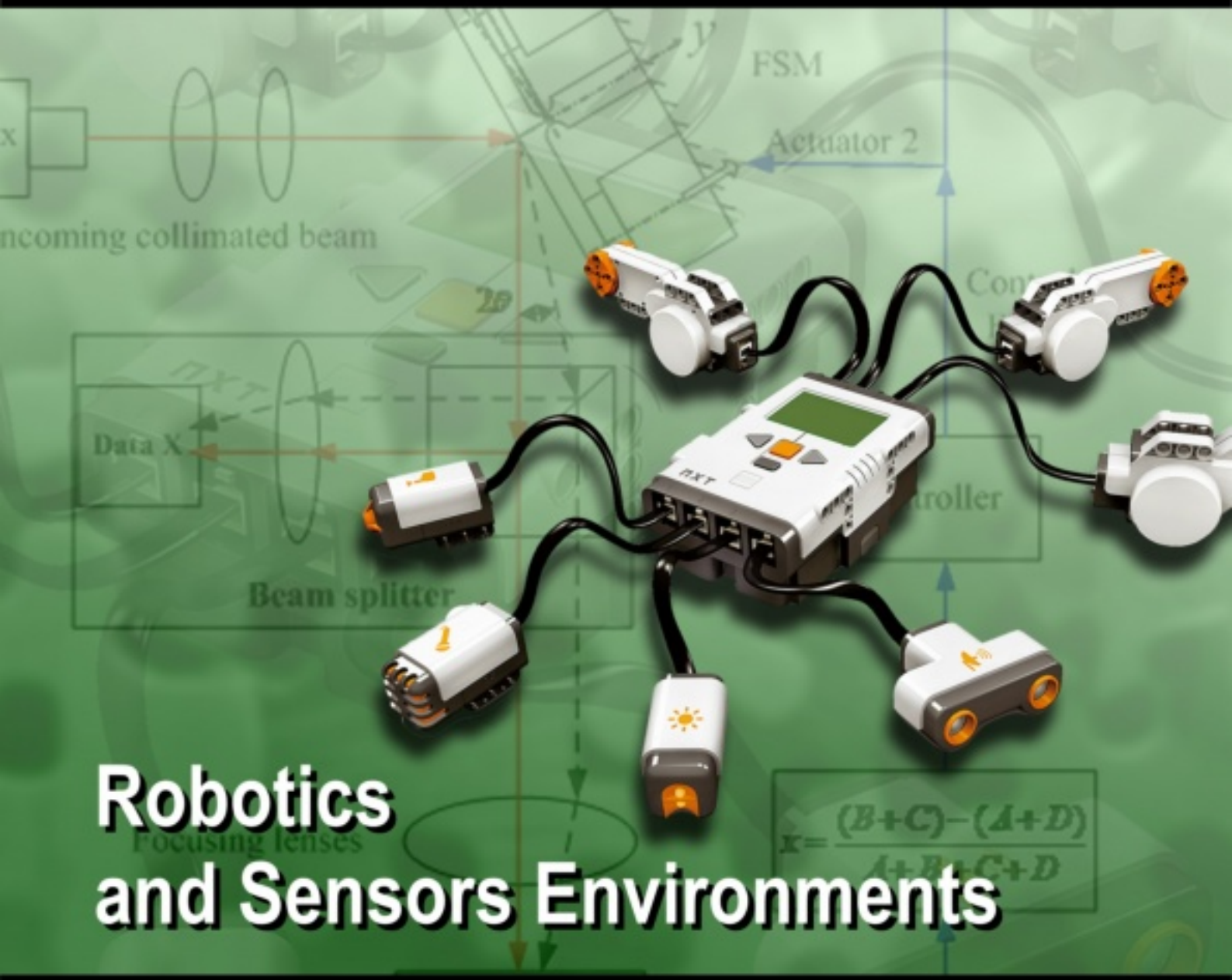

Robotics and Sensors Environments

International Frequency Sensor Association Publishing

IFSA

Sensors & Transducers

Volume 4, Special Issue
March 2009

www.sensorsportal.com

ISSN 1726-5479

Sensors & Transducers Journal (ISSN 1726-5479) is a peer review international journal published monthly online by International Frequency Sensor Association (IFSA).
Available in electronic and CD-ROM.

Sensors & Transducers Journal

Contents

Volume 5
Special Issue
March 2009

www.sensorsportal.com

ISSN 1726-5479

Research Articles

Authors are encouraged to submit article in MS Word (doc) and Acrobat (pdf) formats by e-mail: editor@sensorsportal.com
Please visit journal's webpage with preparation instructions: http://www.sensorsportal.com/HTML/DIGEST/Submition.htm

Sensors & Transducers Journal, Vol. 5, Special Issue, March 2009, pp. 119-134

Sensors & Transducers

ISSN 1726-5479

http://www.sensorsportal.com

Neural Gas and Growing Neural Gas Networks for Selective 3D Sensing: a Comparative Study

Ana-Maria CRETU, Pierre PAYEUR and Emil M. PETRIU
School of Information Technology and Engineering, University of Ottawa
800 King Edward, Ottawa, ON, Canada, K1N 6N5
Tel.: 613-562-5800
E-Mail: {acretu, ppayeur, petriu}@site.uottawa.ca

Received: 30 January 2009 /Accepted: 20 February 2009 /Published: 23 March 2009

Abstract: This paper addresses the topic of intelligent sensing for advanced robotic applications. It is a continuation of our research in the realm of automatic selection of regions of observation for fixed and mobile sensors, directed at innovative approaches to collect only relevant measurements without human guidance. The growing neural gas network solution proposed here for adaptively selecting regions of interest for additional sampling from a cloud of sparsely collected 3D measurements provides several advantages over the previous neural gas solution in terms of user intervention, size of resulting scan and training time. Experimental results and a comparative analysis are presented in the context of selective vision sampling. *Copyright © 2009 IFSA.*

Keywords: Selective sensing, 3D vision, Neural gas network, Growing neural gas network, Feature detection.

1. Introduction

The current generation of 3D data acquisition devices is capable to collect a large amount of data in a relatively limited time. However, the size and the complexity of the dataset frequently represent impediments for the processing of the collected data at a reasonable computational cost. From here stems the interest into finding appropriate procedures that minimize the number of samples by selecting only those points that are relevant for the characteristics of the studied object.

The majority of publications that address the topic of reducing the size and complexity of large datasets post-process the data obtained by the acquisition equipment. This procedure is frequently

based on the users' input on several parameters such as the desired density of sampling, the regularity of sampling, or the minimum distance between data samples. The selection of appropriate values for these parameters is not trivial, as users are seldom aware of the required level of accuracy for a dataset to be further processed for a given application. The development of online automated selective procedures to perform only relevant measurements for the objects under study, ideally without user input, is one of the key techniques expected to bring significant improvement over its post-processing counterpart.

The work presented in this paper constitutes an extension to our previous research on automatic guidance of vision sensors to collect only relevant measurements with limited human intervention. To prevent a large amount of data from being collected and the associated excessive processing load, the proposed framework advantageously employs self-organizing architectures to identify relevant regions of interest in 3D point-clouds during the acquisition procedure. The final result is a multi-resolution point-cloud with a higher resolution in those areas of interest that contain geometrical features. The growing neural gas solution introduced here represents an improvement over our previously proposed neural gas solution in terms of training time, multi-resolution point-cloud size, as well as user intervention.

The paper starts with a brief literature review on the topic of sampling and post-processing of large datasets in Section 2. The proposed framework for selective sensing based on self-organizing architectures is detailed in Section 3. Experimental results for data sampling using vision sensors are shown in Section 4. Section 5 analyses the experimental results obtained with the new method, in comparison with the previous solution based on a neural gas network, as well as with the results obtained using classical uniform and random sampling.

2. Literature Review

Uniform sampling and random sampling are the most popular sampling policies proposed in the literature. The uniform sampling method can be easily implemented and ensures complete coverage of the surface within the sensor's field of view. Samples are spread such that the probability of a surface point to be sampled is equal for all surface points. Its cost can be however high, since the sampling density must be uniformly high everywhere in order to achieve adequate sampling density over those regions requiring the highest resolution. In random sampling, each point of the object has an equal chance of being selected, but only a lower number of points are collected. As the percentage of sampled points increases, the cost gets higher to eventually reach the one of uniform sampling. A risk frequently encountered with random sampling is that samples randomly collected miss important features of the object under study.

Another sampling procedure proposed in the literature is stratified sampling. The technique is based on a subdivision of the sampling domain into non-overlapping partitions. Evenly spaced samples are then collected independently from each partition, therefore ensuring that an adequate sampling is applied to all partitions. A similar idea of a subdivision into cells and replacement of the sample points that fall into the same cell by a common representative is often used in the context of post-processing of large point-clouds or meshes [1-7].

The 3D model proposed by Nehab *et al.* [1] is first voxelized with an octree and a sample is outputed for each voxel. The common representative for a voxel is selected according to a probability that decays as the distance of the sample to the center of the voxel increases. The user controls the sampling resolution, the regularity of the sampling, and the minimum distance between samples. In [2] the representative point for each voxel is the measured point that is closest to the average of points that fall into the same voxel.

The 3D grids proposed by Lee *et al.* [3] are octrees that voxelize 3D points constructed by registration and integration of multiple scanned datasets of an object or scene of objects. The method uses point normal values on the surface of the object, computed based on the knowledge that scanned lines and points are ordered due to the raster scanning procedure employed, and based on a triangulation performed on two neighboring scan lines. Non-uniform grids are then generated using the standard deviation of normal values. The representative point for each grid is the point whose normal is closest to the average of the points in the same voxel.

The standard volumetric subdivision strategy cannot be adapted to non-uniformities in the sampling distribution and sometimes joins unconnected parts of a surface if the grid cells are too large. To alleviate these problems, Pauly *et al.* [4] perform surface-based clustering, where clusters are built by collecting neighboring samples while taking into account local sampling density. Points are incrementally added to a cluster until a maximum size and/or a maximum allowed variation is reached. The sample points of those clusters that do not reach the minimum size or variation bound are distributed to the neighboring clusters.

Uesu *et al.* [5] simplify large unstructured meshes by segmenting them into two parts: the boundary of the domain and the interior samples. Each part is then simplified separately, considering proper error bounds. For the boundaries, a surface-simplification algorithm that takes into account the scalar field defined at the vertices is employed, while the interior points are sampled using a *k-d* tree partition of the mesh from which the samples that are outside the boundary, or closer than a certain minimum distance to the boundary are removed. Finally, the simplified domain boundary and scalar field are combined into a complete, simplified mesh using a Delaunay tetrahedralization.

A similar idea is employed by Song and Feng [6] whose point-cloud simplification algorithm starts by identifying and retaining edge boundaries and then removing least important points from the remaining data based on the contribution to the representation of local surface geometry. If the local geometry cannot be reliably reflected by the neighboring points of a point and their associated properties, that point is considered important for defining geometry, otherwise it can be removed. The removal procedure ends once the specified data reduction ratio is reached.

Kalaiah and Varshney [7] propose a scheme to compactly decimate and represent point-clouds using Principal Component Analysis (PCA). The input is pre-processed using an octree and PCA analysis is performed for each cell. Due to the fact that PCA parameters such as orientation, frame, mean, and variance are similar for coherent regions, the node parameters can be classified using clustering and quantization. At run-time, based on the viewpoint, a cut in the octree is determined and each node of the cut is visualized using a Gaussian random generator. Attributes like normals and color are also generated in the same manner.

Based on the fact that sampling algorithms are usually implying a measure of error, the idea of using error propagation neural networks that minimize an error measure seems a good choice to Fiori *et al.* [8], who propose a multilayer-feedforward network for non-uniform image sampling with application to robot motion control. The neural algorithm allows a controller to determine the robot's location within a structured environment based on a digital image sequence coming from a camera. The proposed sampling procedure starts with a number of pixels uniformly distributed over an image, that all become input points in a neural network. Network pruning is then performed on the basis of inputs relevance and therefore the number of inputs is reduced while the mean-squared error is kept below a pre-defined threshold. After pruning, the remaining sampling points are moved toward the high relevance areas based on a radial-basis-function sampling operator.

All of these methods are not meant to be incorporated in the actual sampling procedure, but they rather post-process collected data. An approach to integrate the sampling procedure into the measurement

procedure is proposed by Pai *et al.* [9, 10] in the context of deformable object modeling. The authors use a probing procedure that considers a known mesh of the object under study, as well as a set of parameters such as the maximum force exerted on the object, the maximum probing depth and the number of steps for the deformation measurement. During probing, an algorithm generates the next position and orientation for the probe based on the specified parameters and the mesh of the object under test. It performs at the same time proximity checks and verifies the expected contact location of the probe with the mesh based on line intersection. However, the procedure is not selective and therefore is similar to collecting data for all the points of the mesh.

3. Proposed Framework

The framework proposed in this paper is intended for direct incorporation into the sampling procedure and is depicted in Fig. 1.

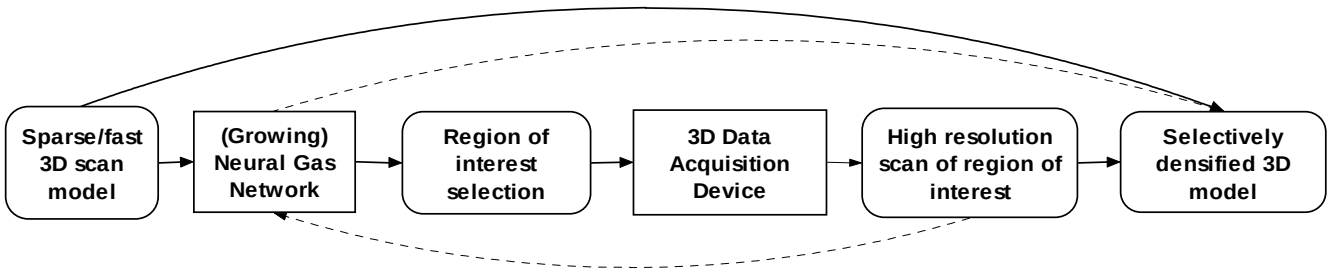

Fig. 1. Proposed framework.

It employs soft computing techniques to achieve automated selective scanning over large workspaces with very limited, ideally without, human intervention. The selective scanning procedure is based on a self-organizing neural map that allows the identification of regions of interest for further refinement from a cloud of 3D sparsely collected measurements. The approach is justified by the ability of self-organizing architectures to quantize the input space into clusters of points with similar properties and therefore easing the identification of those regions where changes in the geometry of the objects under study occur. These areas of changes in the geometry, identified by higher density of points in the self-organizing maps, are the ones that contain features and therefore will be the target of additional scanning.

Starting from an initial low resolution scan of an object, a neural gas network and a growing neural gas network are employed successively, to model the resulting point-cloud. A brief presentation of the characteristics of each of the two networks employed is presented below. Those regions that require additional sampling in order to ensure an accurate model are detected by finding higher density areas in the resulting neural or growing gas map. Rescanning at higher resolution is performed for each identified region and a multi-resolution model is then built using the either the initial sparse model or the resulting neural or growing neural map and augmenting it with the higher resolution scans collected over the regions of interest.

3.1. Neural Gas Networks

The main purpose of the neural gas network is to cluster multi-dimensional vectors. It consists of nodes (cluster centers), which independently move over the data space while learning. The algorithm

starts by initializing the set of network nodes with a predefined number of units whose corresponding reference vectors are chosen randomly according to a probability density function or from a finite set [11, 12]. Each unit has an associated reference vector that indicates its position in the input space. At each training step, the winning neuron that best matches an input vector is identified using the minimum Euclidean distance criterion. The neurons to be adapted in the learning procedure are selected according to their rank. The rank of neurons is the rank they have in an ordered list of distances between their weights and the input vector. A full description of the neural gas algorithm is available in [11].

In the context of this work, the neural gas is employed to model a point-cloud collected during a sparse scan of an object under study with an active range finder. Starting with the points in this point-cloud and an initial configuration of unconnected nodes, the latter move over the data space during adaptation and the model contracts asymptotically towards the points in the input space, respecting their density and taking the shape of the object encoded in the point-cloud.

The work presented here tackles some of the limitations of this neural gas solution introduced in [13], particularly the one related to the predefined number of units of the neural gas map. This size needs to be decided prior to learning and has to be tuned by the user. It also constrains the accuracy of the resulting map. In spite of some guidelines that we developed to choose an appropriate map size based on the size of the initial scan and the desired accuracy of the model, the efficiency of such a solution can vary slightly with the characteristics of the objects considered, such as the size of the object, and the number and the size of the features. Growing networks eliminate this limitation, and are therefore examined in this work to guide the selective sampling procedure and eliminate the need of user intervention.

3.2. Growing Neural Gas Networks

Growing networks add supplementary nodes into the network structure at the position where the accumulated error is the highest and when the number of learning iterations performed is an integer multiple of some predefined value. This eliminates the constraint imposed by the fixed map size of standard neural gas networks. As a node is added, a set of iterations is performed before another new node is added. The growth of the network is terminated when a predefined stopping criterion is met (e.g. a minimum error or a network size limit is reached).

The growing neural gas has no predefined map and builds a topology based on competitive Hebbian learning [14] by inserting an edge between the two closest nodes. Similar to neural gas, the closeness is measured in Euclidian distance from an input signal. The resulting graph is an induced Delaunay triangulation. This induced Delaunay triangulation has been shown to optimally preserve topology in a very general sense [14].

The growing neural gas algorithm can be described as follows [12, 15]: new nodes are added every λ iterations, to support the node with the highest local accumulated error. For each input signal/vector presented to the network, two best matching nodes are selected, whose weights are the closest to the input, based on their Euclidean distance. A neighborhood connection is created between them if the connection does not already exist and its age is set to 0. The position of these nodes and the ones of the topological neighbors of the winner unit are moved such that they better fit the input. All edges that are not used increase in age and if the age exceeds a threshold, a_{max}, the corresponding edges are deleted. Any node that has no edge connection is removed as well. After λ iterations, a new node is added to support the node that has accumulated the highest error in the previous steps. The new node is placed between the node with the highest error and one of its neighbors that has the next highest error. A

global decrease of errors is then performed. The algorithm continues until some stopping criterion is met. The mathematical formulation of the algorithm is presented in detail in [15].

As for the neural gas solution described above, the growing neural gas is employed to detect areas rich in geometrical features. Starting from the points collected during a sparse scan of an object with an active range finder, nodes are added progressively to take the shape of the object encoded in the point-cloud.

3.3. Regions of Interest Detection

Due to the modeling properties of the two networks, higher density areas in the growing neural gas map are related to the existence of 3D features in the object whose point-cloud was provided as input to the networks. A simple technique is employed to detect these higher density regions. A Delaunay triangulation is first applied over the output map in order to connect the nodes of the growing neural gas map. The triangulation is traversed successively and the length of vertices between every pair of points for every triangle is computed. The mean value of all these lengths is estimated and a threshold is set equal to this value. All the vertices longer than the threshold value are then removed from the model. The remaining triangles and associated points identify those regions that require additional sampling. Supplementary data is collected for all these regions and the resulting selectively sampled multi-resolution model is constructed by augmenting either the initial sparse low resolution scan with the higher resolution data samples if a more accurate model is desired; or with by augmenting the (growing) neural gas map with the higher resolution areas if a more compact model is desired. The procedure can be repeated in several steps to improve the final model.

4. Experimental Evaluation

The proposed method based on growing neural gas is tested on sparse 3D data point-clouds of objects, each object presenting different areas of interest, as shown in Fig. 2. Apart from the contour, the area of the head, the neck and the horns correspond to regions of interest for the triceratops model, while the armchair has the edges as regions of interest. For the door model, the regions of interest should be identified around the door knob and the door opening gap.

a) b) c)

Fig. 2. Test objects: a) Toy triceratops, b) foam chair, and c) mock-up car door used for testing.

The normalized data in each point-cloud is provided as input to a growing neural gas map. The results for the toy triceratops are presented in Fig. 3. The full resolution point-cloud contains 12226 points. Fig. 3a shows the enlarged best modeling results for a low resolution initial scan of 3065 points and

Fig. 3b for a medium resolution initial scan of 6113 points of the same triceratops, for $\lambda=3$ and $a_{max}=20$.

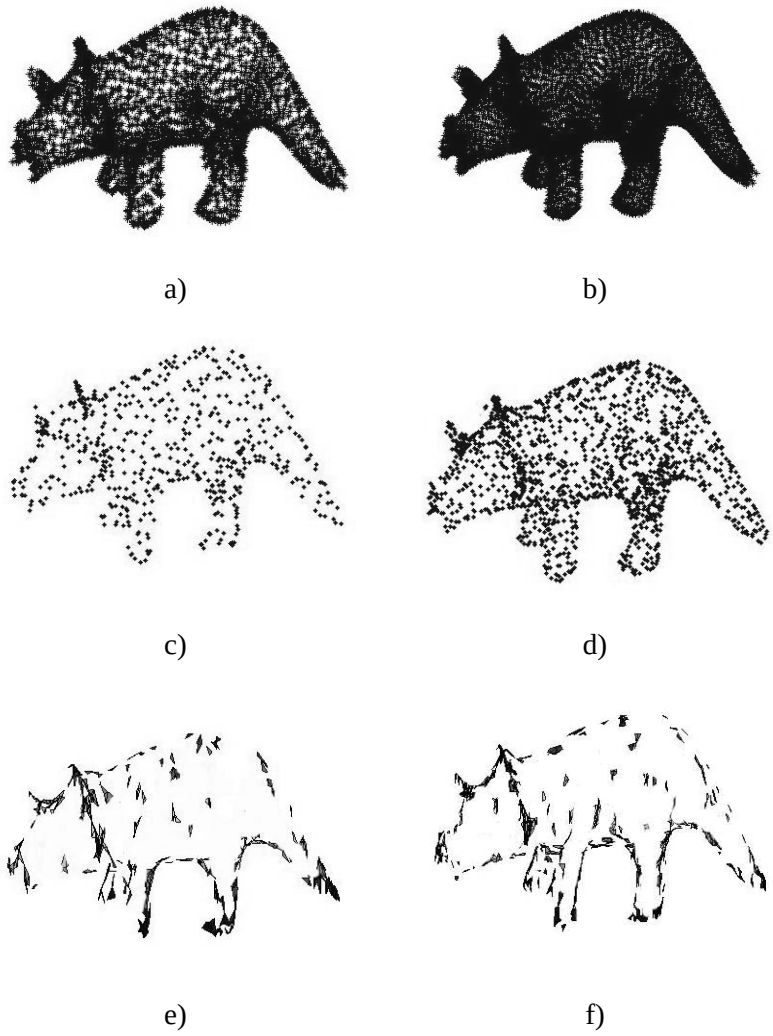

Fig. 3. Initial scan at (a) low resolution (3065 points) and (b) medium resolution (6113 points), growing neural gas model of (c) 757 points and (d) 1410 points, and detected regions of interest for further sampling for (e) low resolution and (f) medium resolution models.

The growing neural gas network (having as inputs these initial sparse point-clouds) builds a topology that respects the density of points in the initial point-cloud. The topology can be seen as a compressed mapping for the initial dataset, as can be observed by comparing Fig. 3a with Fig. 3c for the low resolution model, and Fig. 3b with Fig. 3d for the medium resolution model. The growing neural gas map in Fig. 3c represents a reduction of 94 % when compared to the full resolution point-cloud size, while the map in Fig. 3d corresponds to a reduction of roughly 88.5 % when compared to the full resolution point-cloud size. The areas with dense geometrical features found in these mappings (using the procedure detailed in Section 3.3) are presented in Fig. 3e and Fig. 3f respectively. It can be noticed that the areas dense in features are much better identified and contoured for the higher resolution model, in Fig. 3f. However, in both cases, the network is able to identify, apart from the contours of the model, the areas around the head, the neck and the horns of the triceratops as areas that require additional scanning.

Fig. 4a shows the areas detected for additional scanning framed in a rectangle for the medium resolution model in Fig. 3f. The multi-resolution model built by augmenting the growing neural gas map with the higher resolution areas contains in this case 3165 points and is depicted in Fig. 4b. This selectively densified point-cloud represents a reduction of approximately 75 % from the full resolution point-cloud. The same areas can be identified in the low resolution model where a reduction of approximately 80% can be obtained if augmenting the growing neural gas map with the higher resolution areas. If the high resolution areas are added on the initial sparse scan, the reduction is of roughly 60% from the full resolution point-cloud when the low resolution model is used as a start-point, and of roughly 40% when the medium resolution point-cloud is used to train the growing neural gas network. The multi-resolution point-clouds based on the initial sparse point-cloud are more accurate than their counterpart based on the growing neural gas map, but are denser and therefore larger as well.

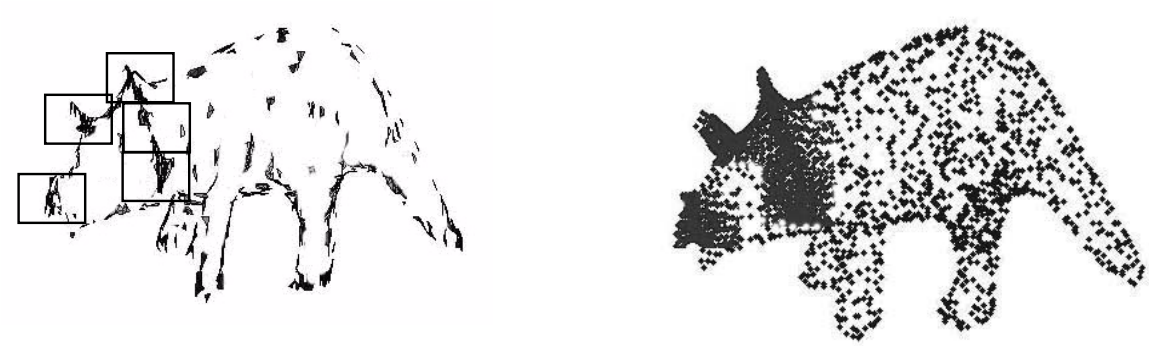

a) b)

Fig. 4. (a) The detected regions of interest on the triceratops model for the medium resolution and (b) the selectively densified point-cloud of the triceratops.

The chair represents an object without many features and its initial dataset contains a raster-like distribution of sampling points. Fig. 5 presents the modeling results using a growing neural gas for a low (3065 points) and a medium (6113 points) resolution initial scans on the chair, obtained for $\lambda=3$ and $a_{max}=20$. The growing neural gas contains 1243 points for the case of the low resolution scan (Fig. 5c) and 2826 points for the medium resolution scan (Fig. 5d).

The detected regions of interest in the growing neural gas map are shown in Fig. 5e and Fig. 5f respectively. As it can be seen, in spite of some noise, the network is able to detect the features in both cases.

As a last example, a fast scan of medium resolution on the mock-up car door is initially performed to obtain the 16384 points medium resolution scan as shown in Fig. 6a. The full high-resolution door model contains 1048576 points.

The resulting growing neural gas map is depicted in Fig. 6b and contains 3750 points. The areas of high density in this map are shown in Fig. 6c, and the multi-resolution point-cloud model of the door in Fig. 6d respectively. The final multi-resolution point-cloud contains 173884 points, which represents a reduction of 83% from the maximum resolution dataset.

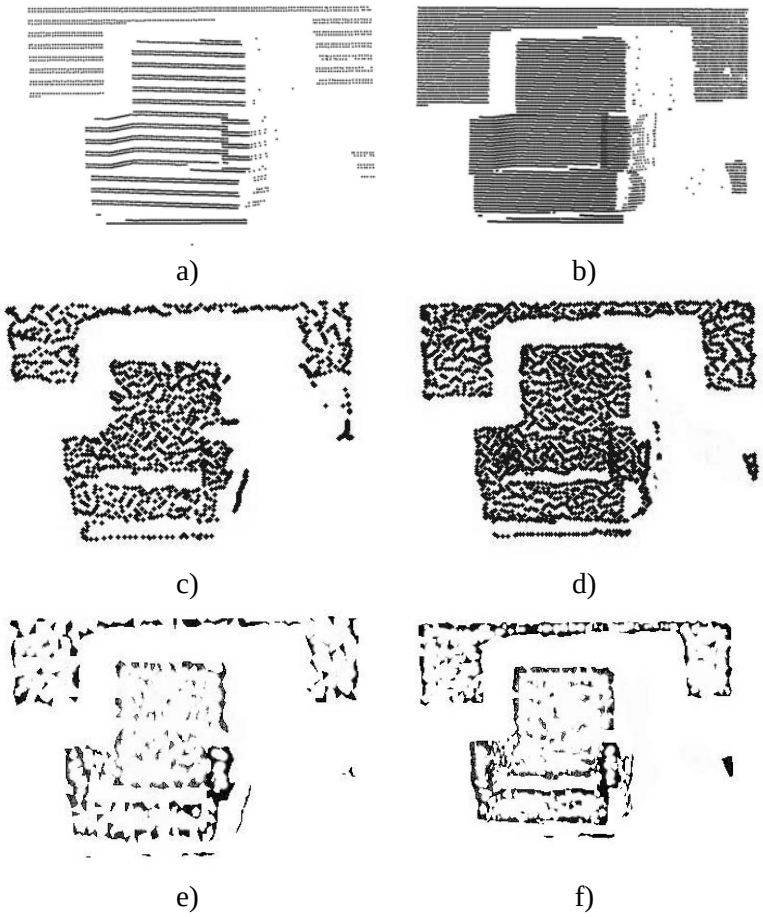

Fig. 5. Initial scan at (a) low resolution and (b) medium resolution, growing neural gas model of (c) 1243 points and (d) 2826 points, and detected regions of interest for further sampling from (e) the low resolution and (f) the medium resolution models.

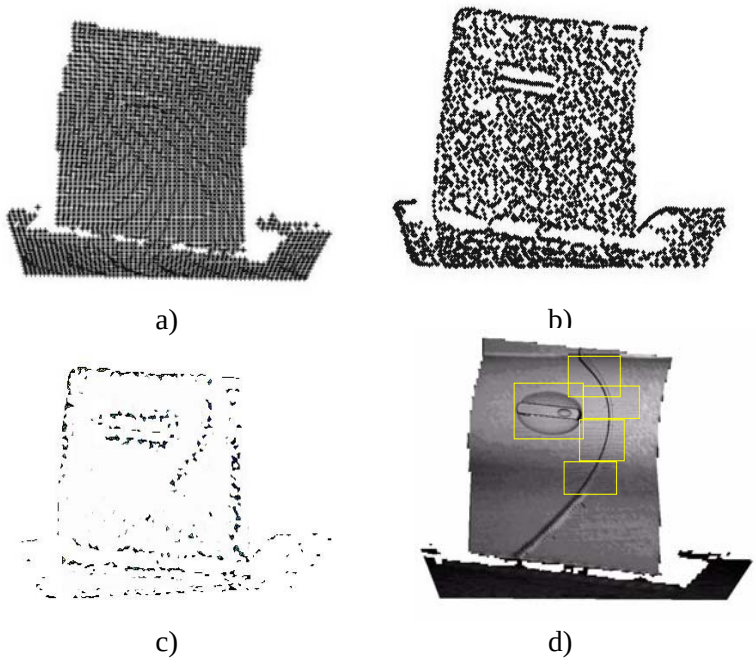

Fig. 6. The mock-up door: (a) 16384 elements point-cloud, (b) growing neural gas map of 3750 points, (c) selected high density areas, and (d) selectively densified point-cloud of 173884 points.

The same procedure can be repeated for each of the regions of interest detected in the previous step. Each region is provided as an individual input to a growing neural gas network in order to further detect fine details that are worth to be scanned at a higher resolution. Fig. 7 presents the details of the higher resolution rendered model of the door for the five selected regions in the previous step. For each of the selected regions it shows the growing neural gas model for $\lambda=3$ and $a_{max}=20$ and the regions of interest detected at the second stage for further scanning, identified as high density areas in the growing neural gas model.

All the presented examples show the capability of the growing neural gas map to capture the fine details in the sparsely collected point-clouds of all the objects under study. By finding the higher density areas in the growing neural gas map, the proposed selective sampling procedure is able to identify and guide the vision sensor to collect only measurements in those regions that are of interest for the improvement of accuracy of the final multi-resolution models.

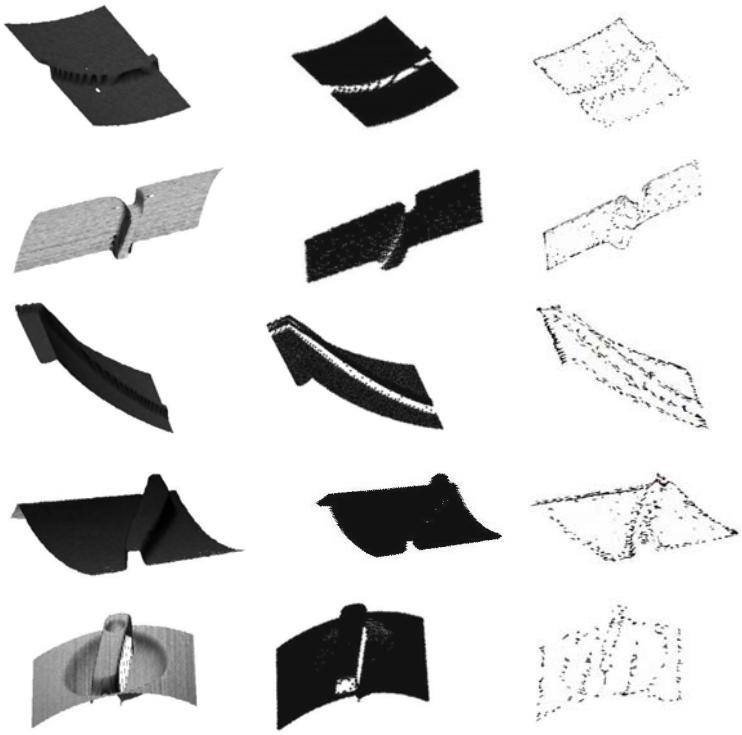

Fig. 7. Different views of rendered selected regions (first column), point-clouds of selected regions (second column), and detected regions of interest for each view (third column).

5. Comparisons with Classic Sampling Algorithms and between Neural Gas and Growing Neural Gas Solutions

To validate the proposed approach, the neural gas and growing neural gas sampling results are first compared with two classical sampling solutions: the uniform sampling and the random sampling. In order to perform the comparison, the same sparse scan of an object is used as a starting point. A growing and a standard neural gas adaptations, a uniform sampling and a random sampling algorithms are applied successively on this scan. To ensure a common basis for comparison, a similar number of points is imposed at the output for each algorithm.

Fig. 8 shows the results of the comparison for the toy triceratops. The initial sparse point-cloud of the toy triceratops of 6113 points, depicted in Fig. 8a, is provided as input to a growing neural gas with

$\lambda=2$ and $a_{max}=20$. Fig. 8b shows the 1427 point map obtained after the adaptation. Therefore the output for all other methods is constrained to 1400-1500 points. Fig. 8c depicts the neural gas map of 1485 points (equivalent to a predefined map of 33×45) obtained after the adaptation over the same sparse scan. Fig. 8d shows the set of 1528 uniformly sampled points from the same initial scan, while an equal set of 1528 randomly sampled points from the initial scan is shown in Fig. 8e. By comparing Fig. 8b and 8c to Fig. 8d and 8e it can be observed that, due to their modeling properties, both the neural gas and the growing neural gas characterize better the features of the object under study when an approximately identical number of samples is imposed at the output of each sampling algorithm. Both self-organizing architectures provide a clearer definition of the area around the neck and the horns of the triceratops than the uniform and the random sampling.

Another set of experiments is conducted without constraining the number of points at the output. Using the same initial scan, experiments are performed for growing neural gas, neural gas, uniform and random sampling, until some reasonably good modeling results are obtained for all the sampling techniques under study. The comparison is based in this case on the minimum number of points that are required for each sampling method to capture the features of the object. This comparison leads to the conclusion that about 1425 points in the neural gas map and growing neural gas map allow for the visual identification of all the features in the model, while approximately double number of points, that is over 3000 points, are required for the uniform and random sampling techniques to capture the same features in the triceratops point-cloud. This experiment shows that the neural gas and growing neural gas provide more compact results, which is a clear advantage in the context of selective sampling.

Moreover, due to their ability to localize features, both the neural gas and the growing neural gas map constitute a good basis to identify the bounded regions of interest in the scan in order to guide the sensors for additional scanning, while the uniform and the random sampling do not possess such properties. All these aspects demonstrate that the use of both neural gas and growing neural gas is appropriate in the context of selective sampling and that both perform better than classical sampling algorithms.

In spite of the fact that neural gas and growing neural gas are both self-organizing architectures with similar approaches and are based on the same ideas, the two techniques present several differences in terms of required user intervention, accuracy of results, training time and remaining errors. To begin with, the growing neural gas eliminates the need for the map size to be decided prior to learning as with the neural gas. Moreover, by comparing the final map size obtained with the growing neural gas with that of the neural gas, it can be seen in Table 1 that the size of the growing neural gas map (i.e. the number of nodes in the resulting graph) is generally smaller than the one required by a neural gas in order to obtain similar modeling results. The description of the results of neural gas network for the same objects is available in [13].

Table 1. Approximate network map sizes for different sizes of initial scans with neural gas (NG) and growing neural gas (GNG) as a function of the number of points in the initial scan, *N*.

Size of initial point-cloud (number of points, *N*)	**Approximate map size with NG**	**Approximate map size with GNG**
2000-3000	60%-100%N	20-45%N
3000-4000	50%-90%N	20-45%N
4000-5000	30%-70%N	20-45%N
5000-6000	20%-60%N	16-49%N
6000-7000	15%-50%N	16-49%N
over 16000	10%-40%N	10-40%N

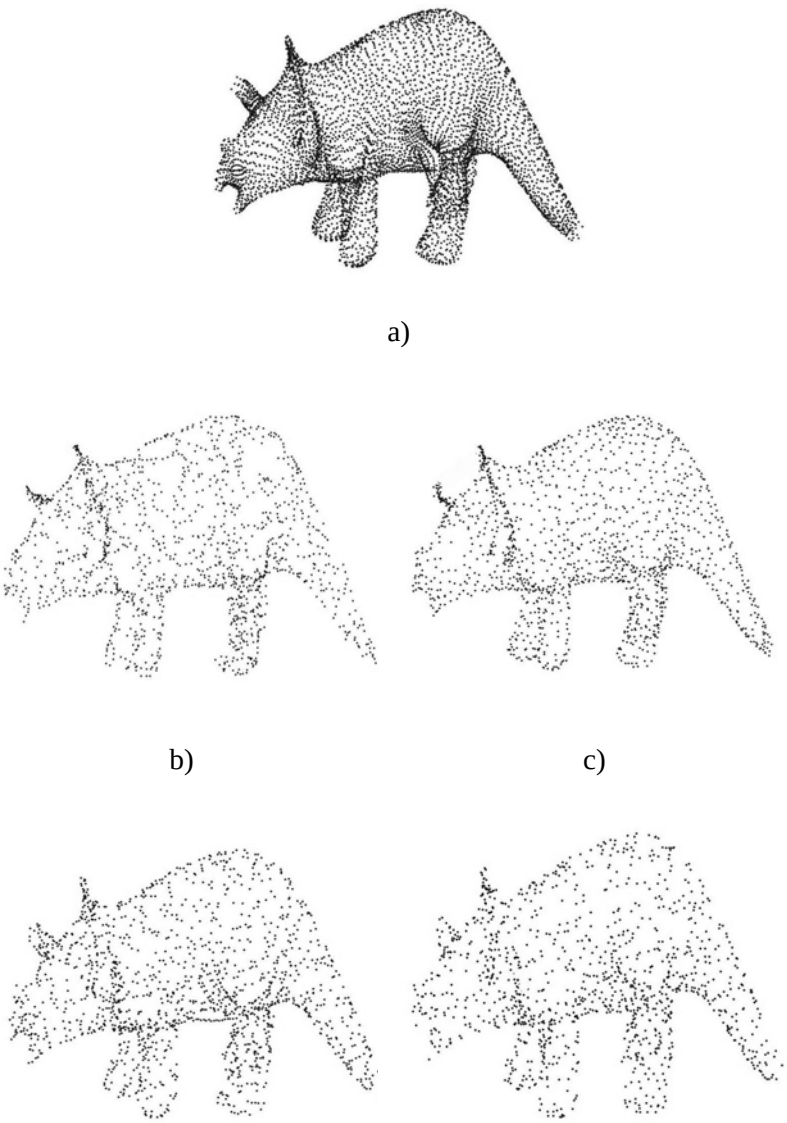

a)

b) c)

d) e)

Fig. 8. Comparison of neural gas map with classical sampling techniques: a) initial sparse point-cloud (6113 points), b) growing neural gas map (1427 points), c) neural gas map (1485 points), d) uniform sampling results (1528 points), and e) random sampling results (1528 points).

The average network map sizes for different initial scans, computed as the average value of the network map sizes for the range of values that provide reasonably good modeling results and for all the objects under study, as per Table 1, are shown in Fig. 9.

The “reasonably good” modeling results are identified as those compressed models with the highest compression rate that offer at the same time an optimal balance between the quality of the model and the time required for training. The quality of the model is monitored from a low average error and good visual distribution of samples over the object surface. The relative error is computed as an average Euclidean distance between each data vector and its winning neuron. As such it shows how close the modeled data is to the initial scan point-cloud. The average error is computed as the average relative error for all objects under study, as in the case of the network map size. Fig. 10 shows the comparison between the growing neural gas and the neural gas in terms of average error.

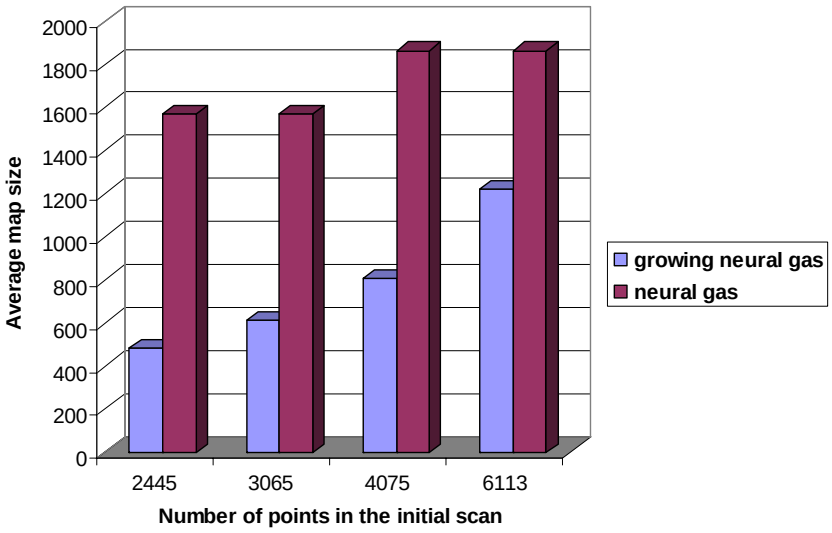

Fig. 9. Comparison between growing neural gas and neural gas based on map size.

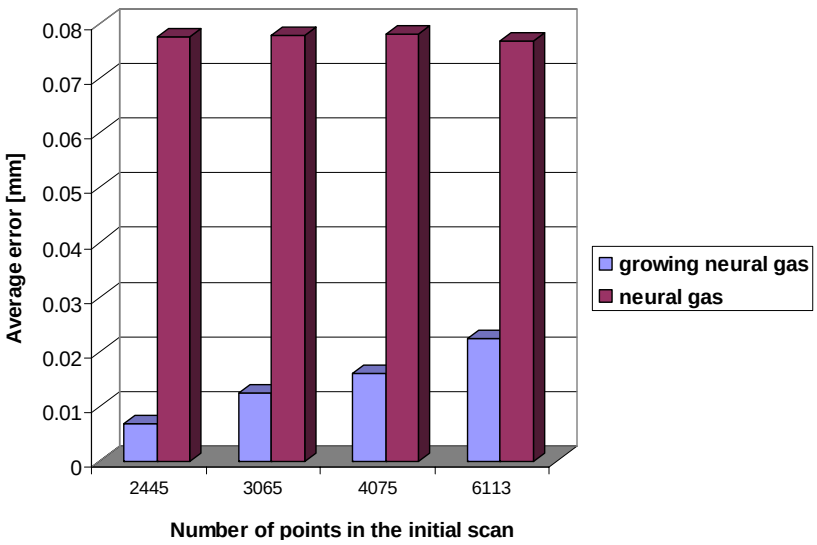

Fig. 10. Comparison between growing neural gas and neural gas based on average error.

As it can be noticed, in spite of the lower network map size, the accuracy of growing neural gas models is higher in comparison to the neural gas counterpart. In terms of training time, the time required to build the model is also generally lower for the growing neural gas, as shown in Fig. 11.

However, since the map obtained with growing neural gas is evenly distributed over raster-like object point-clouds, the relevant areas for additional scanning are slightly harder to identify and they result in higher noise in the characterization of relevant features, as it can be seen in Fig. 12. The first row of presents the best modeling results for the neural gas while the second row presents the growing neural gas models. When comparing the results in Fig. 12, it can be noticed that the edges are clearer around the contours in Fig. 12a - 12c, representing the areas with higher density of geometrical features as detected in the neural gas map, than those in Fig. 12d - 12f that represent the higher density areas detected in the growing neural gas map. Therefore, the results in the second row are slightly noisier.

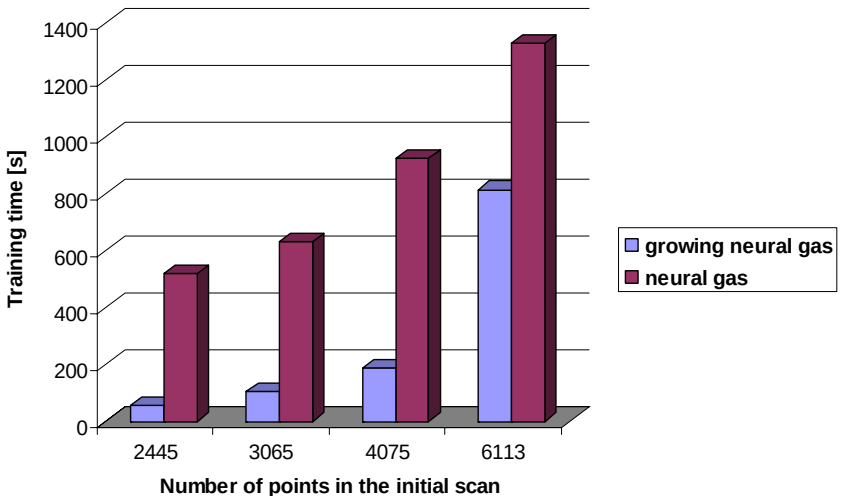

Fig. 11. Comparison between growing neural gas and neural gas based on training time.

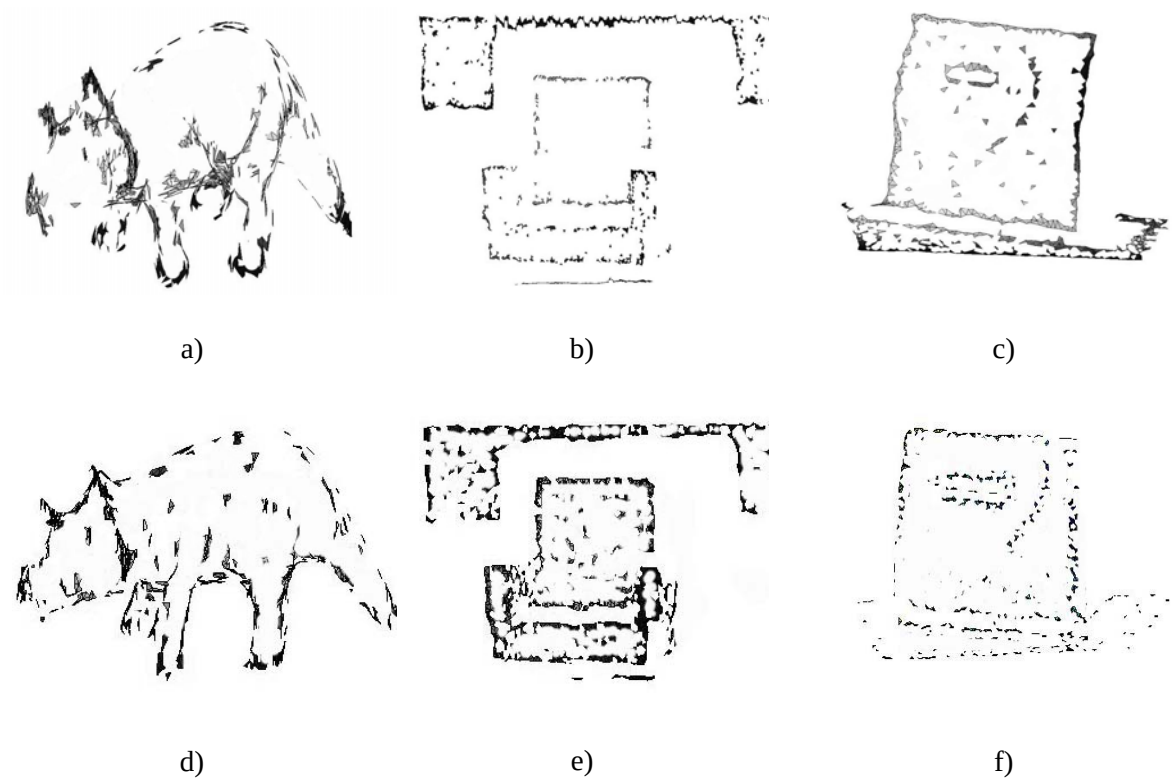

Fig. 12. Higher feature density areas identified in the neural gas map (first row) for (a) triceratops (b) chair and (c) door, and in the growing neural gas map (second row) for (d) triceratops, (e) chair and (f) door.

This phenomenon is alleviated in the case of neural gas model by slightly over-sizing the map dimensions and stopping the adaptation early enough not to allow the output space to become evenly distributed. Such a mechanism is impossible to be established in the case of growing neural gas as the points in the output space are added iteratively to support the node that has accumulated the highest error in the previous steps. The new node is placed between the node with the highest error and the one of its neighbors with the next highest error. Therefore the error between the input space and the map being built is progressively decreased. This involves that the model will respect the density of points in the point-cloud and cover evenly the input space, but gives less control on the training duration.

From this extended experimentation, the growing neural gas reveals to be faster, to lead to lower errors in the mapping and to require less user interaction during the modeling procedure. However it gives slightly noisier results for geometrical feature detection as required for the selection of additional sampling regions. These properties make the growing neural gas an appropriate choice when more compact object models are desired, and when the user is not willing or qualified to interfere in the modeling procedure. On the other hand, neural gas provides clearer definition of the regions that require additional scanning, especially on the edges but requires some trial-and-error settings in order to provide the best results. Therefore this choice is appropriate when the user is interested in accurately finding features over the objects and is prepared to provide an estimate for the adequate map size.

5. Conclusions

The growing neural gas eliminates the need of the map size to be decided prior to learning, as in the case of neural gas. During adaptation, the network adds iteratively nodes to the structure to better fit the data provided as input. The network is capable to capture the fine details and identify the regions in the sparsely collected point-clouds of the objects under study. By finding the high density areas in the growing neural gas map, the proposed selective sampling procedure is able to automatically identify and guide the vision sensors to collect only measurements in those regions that are of interest for the improvement of accuracy of the obtained models, saving at the same time large amount of less relevant data in the scans. The growing neural gas solution is faster, reaches lower errors and does not require user intervention for the selection of an appropriate map size when compared to the previously proposed neural gas solution. Further research is directed towards the use of the growing neural gas network for deformable objects sampling.

References

[1]. D. Nehab, P. Shilane, Stratified Point Sampling of 3D Models, in *Proceedings of the Eurographics Symposium on Point-Based Graphics*, M. Alexa, S. Rusinkiewicz (Eds.), 2004, pp. 49-56.

[2]. R. Dillmann, S. Vogt, A. Zilker, Data Reduction for Optical 3D Inspection in Automotive Applications, in *Proceedings of the IEEE International Conference on Multi-Sensor Fusion and Integration for Intelligent Systems,* 1999, pp. 159-164.

[3]. K. Lee, H. Woo, T. Suk, Point Data Reduction Using 3D Grids, *International Journal of Advanced Manufacturing Technologies,* Vol. 18, 2001, pp. 201-210.

[4]. M. Pauly, M. Gross, L. P. Kobbelt, Efficient Simplification of Point-Sampled Surfaces, in *Proceedings of the IEEE Conference on Visualization*, 2002, pp. 163-170.

[5]. D. Uesu, L. Bavoil, S. Fleishman, J. Shepherd, C. T. Silva, Simplification of Unstructured Tetrahedral Meshes by Point Sampling, in *Proceedings of the IEEE International Workshop on Volume Graphics*, E. Gröller, I. Fujishiro (Eds.), 2005, pp. 157- 238.

[6]. H. Song, H.-Y. Feng, A Point Cloud Simplification Algorithm for Mechanical Part Inspection, Information Technology for Balanced Manufacturing Systems, W. Shen (Ed.), *Springer*, 2006, pp. 461-468.

[7]. A. Kalaiah, A. Varshney, Statistical Point Geometry, in *Proceedings of the Eurographics Symposium on Geometry Processing*, K. Kobbelt, P. Schroder, H. Hoppe (Eds.), 2003, pp. 107 - 115.

[8]. S. Fiori, A. Faustini, P. Burrascano, Non-Uniform Sampling for Robot Motion Control by the GFS Neural Algorithm, in *Proceedings of IEEE International Conference on Neural Networks*, 1999, pp. 2057-2060.

[9]. D. K. Pai, K. van den Doel, D. L. James, J. Lang, J. E. Lloyd, J. L. Richmond, S. H. Yau, Scanning Physical Interaction Behavior of 3D Objects, in *Proceedings of the Conference on Computer Graphics and Interactive Techniques,* 2001, pp. 87-96.

[10].J. Lang, D. K. Pai, R. J. Woodham, Acquisition of Elastic Models for Interactive Simulation, *International Journal of Robotics Research*, Vol. 21, No. 8, 2002, pp.713-733.

[11].M. Martinetz, S. G. Berkovich, K. J. Schulten, Neural-Gas Network for Vector Quantization and its Application to Time-Series Prediction, *IEEE Transactions on Neural Networks*, Vol. 4, No. 4, 1993, pp. 558-568.

[12].B. Fritzke, Some Competitive Learning Methods, draft, 1997, [Online]. http:www.neuroinformatik.ruhr-unibochum.de/ini/VDM/research/gsn/JavaPaper/

[13].A.-M. Cretu, P. Payeur, E. M. Petriu, Selective Vision Sampling with Neural Gas Networks, in *Proceedings of the IEEE International Instrumentation and Measurement Technology Conference*, Victoria, Canada, 2008, pp. 478-483.

[14].T. M. Martinetz, Competitive Hebbian Learning Rule Forms Perfectly Topology Preserving Maps, in *Proceedings of the International Conference on Artificial Neural Networks,* Springer, Amsterdam, 1993, pp. 427-434.

[15].B. Fritzke, Unsupervised Ontogenic Networks, in Handbook of Neural Computation, Eds. E. Fiesler, R. Beale, *IOP Publishing Ltd and Oxford University Press*, 1997, C2.4.

Guide for Contributors

Aims and Scope

Sensors & Transducers Journal (ISSN 1726-5479) provides an advanced forum for the science and technology of physical, chemical sensors and biosensors. It publishes state-of-the-art reviews, regular research and application specific papers, short notes, letters to Editor and sensors related books reviews as well as academic, practical and commercial information of interest to its readership. Because it is an open access, peer review international journal, papers rapidly published in *Sensors & Transducers Journal* will receive a very high publicity. The journal is published monthly as twelve issues per annual by International Frequency Association (IFSA). In additional, some special sponsored and conference issues published annually.

Topics Covered

Contributions are invited on all aspects of research, development and application of the science and technology of sensors, transducers and sensor instrumentations. Topics include, but are not restricted to:

- Physical, chemical and biosensors;
- Digital, frequency, period, duty-cycle, time interval, PWM, pulse number output sensors and transducers;
- Theory, principles, effects, design, standardization and modeling;
- Smart sensors and systems;
- Sensor instrumentation;
- Virtual instruments;
- Sensors interfaces, buses and networks;
- Signal processing;
- Frequency (period, duty-cycle)-to-digital converters, ADC;
- Technologies and materials;
- Nanosensors;
- Microsystems;
- Applications.

Submission of papers

Articles should be written in English. Authors are invited to submit by e-mail editor@sensorsportal.com 6-14 pages article (including abstract, illustrations (color or grayscale), photos and references) in both: MS Word (doc) and Acrobat (pdf) formats. Detailed preparation instructions, paper example and template of manuscript are available from the journal's webpage: http://www.sensorsportal.com/HTML/DIGEST/Submition.htm Authors must follow the instructions strictly when submitting their manuscripts.

Advertising Information

Advertising orders and enquires may be sent to sales@sensorsportal.com Please download also our media kit: http://www.sensorsportal.com/DOWNLOADS/Media_Kit_2008.pdf